HEAT-REJECTION AND WEIGHT CHARACTERISTICS OF FIN-TUBE SPACE RADIATORS WITH TAPERED FINS

by

Henry C. Haller
Lewis Research Center

Gordon C. Wesling
General Electric Company

Seymour Lieblein
Lewis Research Center

NATIONAL AERONAUTICS AND SPACE ADMINISTRATION • WASHINGTON, D. C. • FEBRUARY 1964

HEAT-REJECTION AND WEIGHT CHARACTERISTICS OF FIN-TUBE SPACE RADIATORS WITH TAPERED FINS

By

Henry C. Haller

Lewis Research Center
Cleveland, Ohio

Gordon C. Wesling

General Electric Company
Cincinnati, Ohio

and

Seymour Lieblein

Lewis Research Center
Cleveland, Ohio

NATIONAL AERONAUTICS AND SPACE ADMINISTRATION

For sale by the Office of Technical Services, Department of Commerce,
Washington, D.C. 20230 -- Price $1.00

HEAT-REJECTION AND WEIGHT CHARACTERISTICS OF FIN-TUBE SPACE RADIATORS WITH TAPERED FINS

By Henry C. Haller, Gordon C. Wesling, and Seymour Lieblein

Lewis Research Center

SUMMARY

An analysis was made of the radiant blackbody heat-rejection and weight characteristics of a direct-condensing radiator with a linearly tapered fin between two tubes. Considered in the analysis are such factors as tube armor protection, mutual irradiation occurring between the fin and the adjoining tube surfaces, and fin base thickness and taper angle. Results of the thermal analysis for three fin tapers are presented in terms of a conductance parameter involving a comparison of the radiation capability of a fin with its heat conducting capability, the ratio of fin tip to base thickness, the ratio of tube outside radius to fin length, and the ratio of fin base thickness to fin length. For practical configurations, the effects of fin base thickness and taper angle on total heat transfer are negligible.

The weight-minimization procedure used in this analysis substantiated the fact that the maximum heat rejection per unit weight occurs at conductance parameters approximately equal to 1 with tapered as well as with constant-thickness fins. For minimum weight, the tapered fin is thicker at the root and is longer than the corresponding minimum-weight constant-thickness fin. The advantages gained by tapered fins are highly dependent on the choice of required armor protection, material, heat-rejection load, and surface temperature. For the illustrative calculations considered, in which a 1-megawatt-system radiator at 1700° R with a 0.90 probability of no punctures in 500 days was prescribed, fin tapering results in a maximum weight saving of 10 percent for a triangular fin as compared to a constant-thickness fin. A similar result was obtained for a radiator operating at 1160° R for a 30-kilowatt system. The effect of fin tapering on radiator planform area was also investigated. Results indicate that an increase in planform area occurs with increasing fin taper at conditions of maximum heat rejection per unit weight. These conclusions are based on fin and tube heat transfer without consideration of the fluid pressure drop or the header weight contributions that may decrease the indicated advantages of tapering.

INTRODUCTION

A major problem in the design of closed-cycle space powerplants is the rejection of large amounts of energy by radiation. Several studies indicate that

the meteoroid-protected radiator may be the heaviest component of a space power system, and weight optimization is of prime importance for heat-rejection systems in space (refs. 1 to 3). The use of fin surfaces between fluid-carrying tubes has been recognized as a practical design concept for reducing radiator weight. The characteristics of radiating fin surfaces of several configurations have been presented in a number of papers (e.g., refs. 4 to 6). The investigations presented in references 5 and 6 show that linearly tapered fins have greater ratios of heat rejection to weight than fins of constant thickness and approach the minimum-weight cusp profile analyzed in references 7 and 8.

The purpose of this report is to analyze the heat-rejection and weight characteristics of central-fin-tube radiators incorporating linearly tapered fins and to identify potential weight savings over radiators with fins of rectangular profile. The analysis considers the radiant interaction between tube and fin surfaces and the total weights of both fins and tubes. The first part of the analysis applies the principles of reference 9 to heat rejection from a fin-tube radiator with linearly tapered central fins. The second part considers the overall ratio of heat rejection to radiator weight for several applications of interest. The radiator weight includes armor to protect the primary tubes from meteoroid penetration as recommended in reference 10, but it does not include inlet or outlet headers.

The heat-rejection analysis is carried out for the situation where the fin and the tube are of infinite length in the direction normal to the cross section of the tube. The analysis treats fins having various degrees of linear taper, various ratios of tube outside radius to fin half-length, and a range of dimensionless conductance parameters. The minimum-weight cusp-profile fin was not treated in the analysis presented herein.

SYMBOLS

A	surface area, sq ft
A_V	vulnerable area, sq ft
A^*	planform area, sq ft
a	penetration correction factor
c	velocity of sound in material, $\sqrt{\frac{E_a g}{\rho_a}}$, ft/sec
D	tube diameter, ft
E_a	Young's modulus, lb/sq ft
F	angle factor, fraction of energy leaving surface that is incident upon another surface
g	acceleration due to gravity, ft/sec^2

k	thermal conductibity, Btu/(hr)(ft)(^{o}R)
L	half-length of fin, ft
N_c	dimensionless conductance parameter, $\frac{\sigma L^2 T_b^3}{k y_o}$
$P(0)$	probability of zero punctures
$\mathscr{P}_e$	powerplant output, Mw
Q	heat flow, Btu/hr
R	tube radius, ft
T	temperature, ^{o}R
$\overline{V}$	average meteoroid velocity, ft/sec
W	weight, lb
X	normalized distance coordinate, x/L
x	coordinate measuring distance along fin, ft
Y	normalized half-thickness coordinate, y/y_o
Y_l	ratio of fin tip to base thickness, y_l/y_o
y	coordinate measuring half-thickness of fin, ft
y_l	midfin half-thickness, ft
y_o	half-thickness of fin at base, ft
Z	radiator tube length, ft
α,β	constants in penetration formula
δ	tube wall thickness, ft
η	efficiency or effectiveness
η_c	cycle thermal efficiency
θ	normalized temperature, T/T_b
$\dot{\theta}$	slope of temperature profile, $\frac{d\theta}{dX}$
$\overline{\theta}_i$	approximation to θ_i

ρ	density, lb/cu ft unless otherwise specified
σ	Stefan-Boltzmann constant, 0.1713×10^{-8} Btu/(hr)(sq ft)($^{\circ}R^4$)
τ	exposure time, days
$\varphi^*, \varphi^{**}, \psi^*, \psi^{**}, \omega^*$	angles in fig. 1

Subscripts:

a	armor
b	tube base surface
c	tube liner
cond	conduction
f	fin
i	inside
o	outside
p	particle
r	radiator
rad	radiation
x	coordinate measuring distance along fin, ft
1	tube surface 1
2	tube surface 2
3	adjacent fin surface

FIN TEMPERATURE PROFILE

Assumptions

The analysis considers the general case of a linearly tapered fin of length L and taper ratio Y_l attached to a tube with a constant surface temperature T_b. Energy input to the fin comprises heat conduction along the fin from the tube-fin interface and incident radiation from the adjacent tapered fin and the two tube surfaces. Figure 1 shows the geometrical setup used in the analysis of the fin-tube radiator panel, and figure 2 indicates the fin profiles studied.

The specific assumptions used in the development of the fin heat-transfer relations are

(1) The radiator surfaces act as blackbodies with incident and emitted radiation governed by Lambert's cosine law.

(2) Incident radiation from external sources is negligible.

(3) All conditions are constant along the length of the tube.

(4) Heat is radiated from both upper and lower surfaces of the fin and the tube.

(5) The tube surface is at a constant temperature longitudinally and circumferentially.

(6) The heat flow in the fins is steady-state one-dimensional flow, and the fin base is at the temperature of the tube.

(7) Material properties are constant and evaluated at the fin base temperature.

(8) The development of fin and tube angle factors is based on an infinite length of tube and fin.

(9) The fin surface area is based on the length of the fin measured from the centerline of the fin at its base.[1]

Formulation of Equations

When an element of the fin surface in figure 1 is considered and the previous assumptions are employed, the law of energy conservation can be expressed as the energy balance between the net heat transfer due to conduction and radiation:

$$dQ_{cond} + dQ_{rad} = 0 \tag{1}$$

The net internal heat conduction through the element for half of the fin thickness is expressed as

$$dQ_{cond} = \frac{d}{dx}\left(-kyZ\frac{dT}{dx}\right)dx \tag{2}$$

The net radiant heat rejection from the element of area on the upper surface of

[1]The increase in fin surface area due to an increase in fin thickness is less than one-half of 1 percent of the fin length for a practical limiting case given by $y_o/R_o \leq 0.1$, $R_o/L = 1.0$, and $R_o = 1.0$ in.

the fin is composed of its emission minus the incident energy. The emitted energy from the surface element is given by

$$\sigma T^4 \frac{Z}{\cos \omega^*} dx \tag{3}$$

and the incident energy on the element from the tube surfaces and the opposing fin surface is

$$\sigma T_b^4 A_1 F_{1-x} + \sigma T_b^4 A_2 F_{2-x} + \frac{\sigma Z}{\cos \omega^*} \int_L^{2L} T^4 F_{x_3-x} \, dx \tag{4a}$$

where A_1 and A_2 are, respectively, the exposed surface area of the tube quadrants adjacent to the fin surface in question.

For practical fin-tube configurations in which y_o/R_o is generally not greater than 0.10, the amount of energy incident on the fin surface from an opposing fin can be neglected, since the angle factor from the opposing fin to the element on the fin will be considerably less than the angle factors from either tube. The net exchange of energy is made additionally insignificant when it is noted that the average temperature of the portion of the opposing fin that would contribute the most to an element near the fin tip is at the same temperature as the opposing fin. When this energy input is neglected and the reciprocity relations

$$A_1 F_{1-x} = Z \frac{dx}{\cos \omega^*} F_{x-1}$$

and

$$A_2 F_{2-x} = Z \frac{dx}{\cos \omega^*} F_{x-2}$$

are applied to equation (4a), the incident energy expression

$$\frac{\sigma T_b^4 Z}{\cos \omega^*} (F_{x-1} + F_{x-2}) dx \tag{4b}$$

is produced. The net radiation leaving the surface element is then given by

$$dQ_{rad} = \frac{\sigma Z}{\cos \omega^*} \left[T^4 - T_b^4 (F_{x-1} + F_{x-2}) \right] dx \tag{5}$$

and the complete energy balance on the element can be written as

$$\frac{d}{dx} \left(ky \frac{dT}{dx} \right) = \frac{\sigma}{\cos \omega^*} \left[T^4 - T_b^4 (F_{x-1} + F_{x-2}) \right] \tag{6}$$

This differential equation describing the fin temperature distribution can be rewritten in a dimensionless form by introducing the following parameters:

$$\theta = \frac{T}{T_b} \qquad X = \frac{x}{L} \qquad Y = \frac{y}{y_o} = 1 - X(1 - Y_l)$$

In terms of these new variables, equation (6) can be written as

$$\frac{d}{dX}\left(Y \frac{d\theta}{dX}\right) = \frac{N_c}{\cos \omega^*}\left[\theta^4 - (F_{X-1} + F_{X-2})\right] \tag{7a}$$

where

$$N_c = \frac{\sigma L^2 T_b^3}{k y_o} \tag{7b}$$

and

$$\cos \omega^* = \frac{1}{\sqrt{1 + (1 - Y_l)^2 \left(\frac{y_o}{L}\right)^2}} \tag{7c}$$

The angle factors in equation (7a) are evaluated by using a relation (ref. 11, eq. (31-38)) that applies to parallel surfaces of infinite length (i.e., tube and fin length, $Z = \infty$). For the configuration of figure 1 the angle factors are

$$F_{X-1} = \frac{1}{2}(\sin \psi_1^{**} - \sin \psi_1^*) \tag{8a}$$

$$F_{X-1} = \frac{1}{2}(\sin \psi_2^{**} - \sin \psi_2^*) \tag{8b}$$

The evaluation of the angle factors in terms of the parameters X, R_o/L, y_o/L, and y_l/y_o is carried out by using the geometry and the nomenclature of figure 1. The exact expressions developed include the effects of fin thickness and fin taper on the angle factors. The required angles that are used in equations (8a) and (8b) are

$$\psi_1^{**} = \frac{\pi}{2}$$

$$\psi_1^* = \sin^{-1}\left[\frac{\sqrt{\left(\frac{R_o}{L} + X\right)^2 - \left(\frac{R_o}{L}\right)^2}}{\frac{R_o}{L} + X}\right] + \tan^{-1}\left[\frac{y_o}{L}\frac{1 - (1 - Y_l)X}{X + \frac{R_o}{L}}\right] + \sin^{-1}\left[\frac{\frac{y_o}{L}(1 - Y_l)}{\sqrt{1 + (1 - Y_l)^2\left(\frac{y_o}{L}\right)^2}}\right]$$

$$\psi_2^{**} = \frac{\pi}{2} - \sin^{-1}\left[\frac{\frac{y_o}{L}(1 - Y_l)}{\sqrt{1 + (1 - Y_l)^2\left(\frac{y_o}{L}\right)^2}}\right] - \tan^{-1}\left[\frac{y_o}{L}\frac{(1 - Y_l)X}{2 - X}\right]$$

$$\psi_2^{*} = \sin^{-1}\left[\frac{\sqrt{\left(2 - X + \frac{R_o}{L}\right)^2 - \left(\frac{R_o}{L}\right)^2}}{2 - X + \frac{R_o}{L}}\right] + \tan^{-1}\left[\frac{y_o}{L}\frac{1 - (1 - Y_l)X}{2 + \frac{R_o}{L} - X}\right]$$

$$- \sin^{-1}\left[\frac{\frac{y_o}{L}(1 - Y_l)}{\sqrt{1 + \left(\frac{y_o}{L}\right)^2(1 - Y_l)^2}}\right]$$

With the previous formulation for the angle-factor expressions (eqs. (8a) and (8b)), the exact evaluation of the fin energy balance (eq. (7a)) is complete.

Calculated variations of the angle factor from adjacent fin to tube, including the effects of fin thickness and taper ratio as obtained from equation (8a), are shown in figure 3. As expected, fin taper and thickness reduce the angle factor. This comparison indicates that a sizable error in the angle-factor from the entire fin to a tube can result when large fin thicknesses are not accounted for (as in ref. 9). The true measure of the result of neglecting fin thickness and taper angle, however, will depend on the corresponding effects on the net heat transfer.

Computational Procedure

It was necessary to use numerical techniques to solve equation (7a) for $\dot{\theta}_{X=0}$ and for the θ profile from $X = 0$ to $X = 1$. The finite-difference technique used was a form of Kalaba's method. Central finite differences applied to $\frac{d}{dX}\left(Y\frac{d\theta}{dX}\right)$ yield

$$\frac{d}{dX}\left(Y\frac{d\theta}{dX}\right)_i = \frac{(Y\dot{\theta})_{i+\frac{1}{2}} - (Y\dot{\theta})_{i-\frac{1}{2}}}{\Delta X} \tag{9}$$

Applying central differences to $\dot{\theta}$ yields

$$\frac{d}{dX}\left(Y\frac{d\theta}{dX}\right)_i = \frac{Y_{i+\frac{1}{2}}(\theta_{i+1} - \theta_i) - Y_{i-\frac{1}{2}}(\theta_i - \theta_{i-1})}{(\Delta X)^2} \tag{10}$$

The term θ_i^4 was approximated by a finite Taylor series, namely, $\theta_i^4 = \overline{\theta}_i^4 + 4\overline{\theta}_i^3(\theta_i - \overline{\theta}_i)$ or $\theta_i^4 = 4\theta_i\overline{\theta}_i^3 - 3\overline{\theta}_i^4$, where $\overline{\theta}_i$ is an approximation to θ_i. Thus, θ_i^4 becomes a linear function of θ_i.

The finite-difference equations were set up in three-diagonal form, were reduced to two-diagonal form, and were solved by gaussian backward substitution by using an arbitrary initial guess for θ. This process was repeated with the new computed values for θ. Four such iterations yielded an accuracy of ± 1 in the fifth decimal place, or, roughly, each iteration yielded an additional decimal place. An IBM 7090 electronic digital computer was used for the numerical solution.

Results

Each solution of the fin energy equation provided a temperature distribution along the fin. Results are plotted in figures 4(a), (b), and (c) as functions of X for several parametric values of N_c and R_o/L for triangular, trapezoidal, and rectangular fins, respectively. The view factors used to obtain the curves of figure 4 were based on the simplified case of $y_o/L = 0$. The effect of the fin thickness parameter y_o/L on the temperature distribution was calculated to be small for the cases shown in figure 4. A maximum error in θ of 2 percent results at the midpoint of the fin ($X = 1$) for $y_o/R_o = 0.1$, $R_o/L = 1.0$, and large values of N_c. For values of $N_c = 1.0$ (near optimum), the error in neglecting fin thickness is less than 1 percent at these conditions.

The curves of figure 4 exhibit the expected trend of small temperature drops being associated with low values of N_c, and the R_o/L ratio contributes only a minor effect at this condition. As N_c increases, so does the fin temperature drop and the importance of the ratio R_o/L. A comparison of figures 4(a), (b), and (c) shows that increasing the fin taper increases the temperature drop along the fin for fixed values of the conductance parameter and the ratio R_o/L. This is plausible since the fin cross-sectional area at any point on the fin is decreased as the taper is increased, and thus the thermal resistance is increased.

RADIATOR HEAT TRANSFER

Fin Heat Rejection

After the temperature distribution and the slope of the temperature distribution curve at $X = 0$ have been determined, the net heat transferred by the fin can be calculated. The net heat loss from one side of the fin of length L is equivalent to the amount of heat conducted into half of the fin base thickness (fig. 1). Fourier's heat-conduction equation is

$$Q_f = -ky_oZ\left(\frac{dT}{dx}\right)_{x=0} = \frac{-kZy_oT_b}{L}\left(\frac{d\theta}{dX}\right)_{X=0} \tag{11}$$

This equation can be placed in dimensionless form and can be evaluated by using the solutions of the fin energy equation (7a). The comparison of this fin energy rejection to the total heat loss from one side of a black isothermal fin of length L can be expressed as

$$\frac{Q_f}{\sigma L Z T_b^4} = -\frac{1}{N_c}\left(\frac{d\theta}{dX}\right)_{X=0} = \eta_f \tag{12}$$

Equation (12) is the definition for the efficiency of the fin.

For the case of $N_c = 0$ (infinite thermal conductivity and constant temperature), equation (12) is indeterminate. For these conditions, however, the fin efficiency can be found from simple geometrical considerations. Since the heat loss is the difference between emitted and incident energy, the fin efficiency becomes

$$\frac{Q_f}{\sigma L Z T_b^4} = 1 - \int_0^1 (F_{X-1} + F_{X-2})dX \tag{13}$$

Thus, when $R_o/L = 0$, $\eta_f = 1.0$, and when $R_o/L \to \infty$, $\eta_f \to 0$.

Results of the fin efficiency calculations are shown in figure 5 for variations in N_c, R_o/L, and fin taper for the simplifying case of $y_o/L = 0$. Increasing the conductance parameter N_c or the fin taper y_l/y_o decreases the fin efficiency because of the corresponding reductions in the fin temperature profile (fig. 4). For the limiting case when $R_o/L = 0$, there is no radiant interchange between tube and fin. This is the plane fin case that is treated in references 4 and 6. The decrease in η_f with increasing R_o/L is a reflection of the increasing effects of tube occlusion.

If the fin thickness ratio is considered in the fin heat rejection, the fin efficiency as described by equation (12) will increase. This is caused by a reduction in the occlusion of the tube on the fin, which permits a larger amount of energy to escape. Numerical results indicate less than a 2-percent error is incurred in η_f when y_o/L is neglected for the case of $R_o/L = 1.0$, $y_o/R_o = 0.1$, and N_c in the range of interest.

Tube Heat Rejection

The net heat loss from the tube surface is equal to the energy emitted by the exposed tube surface minus the incident radiant flux, which is composed of emission from the fins and the opposing tube surfaces. If one-quarter of the surface of tube 1 in figure 1 is considered, the tube-surface heat loss per unit length of tube can be written as

$$\frac{Q_b}{Z} = \sigma T_b^4 R_o\left[\frac{\pi}{2} - \sin^{-1}\left(\frac{y_o}{R_o}\right)\right]$$

$$- \left\{\int_0^{2L} \frac{\sigma T^4}{\cos \omega^*}(F_{x-1})dx + \sigma T_b^4 R_o\left[\frac{\pi}{2} - \sin^{-1}\left(\frac{y_o}{R_o}\right)\right]F_{2-1}\right\} \qquad (14)$$

Inasmuch as the incident energy from the fin, at $X = 0$ to $X = 1$, to tube 2 is equal to the incident energy from the fin, at $X = 1$ to $X = 2$, to tube 1, the fin-to-tube angle factor in equation (14) can be expressed as

$$\int_0^{2L} F_{x-1}\, dx = \int_0^{L} (F_{x-1} + F_{x-2})dx \qquad (15)$$

The determination of the angle factor from tube 2 to tube 1, including the effect of fin thickness, is obtained from angle-factor algebra and is written as

$$F_{2-1} = 1 - \frac{1}{\frac{\pi}{2} - \sin^{-1}\left(\frac{y_o}{R_o}\right)}\left[1 + \frac{2}{\cos \omega^*}\frac{L}{R_o}\int_0^{L} (F_{x-1} + F_{x-2})dx\right] \qquad (16)$$

Substituting equations (15) and (16) into equation (14), nondimensionalizing, and comparing the actual heat loss Q_b with the ideal emission from the quarter-circle surface of the tube yield

$$\frac{\frac{Q_b}{Z}}{\sigma T_b^4 \frac{\pi R_o}{2}} = \frac{2}{\pi}\left\{1 + \frac{L}{R_o}\left[1 - \frac{1}{\cos \omega^*} + \frac{1}{\cos \omega^*}\int_0^{1} (F_{X-1} + F_{X-2})(2 - \theta^4)dX\right]\right\} = \eta_b \qquad (17)$$

This expression, which is the tube-heat-rejection efficiency, is identical in form to the equation presented in reference 9 with the exception of the $\cos \omega^*$ term, which is a function of the fin taper (eq. (7c)). The effects of fin taper and fin thickness are also introduced in the angle-factor terms F_{X-1} and F_{X-2} obtained from equations (8a) and (b) and from the numerical values of the fin temperature profile $\theta(X)$ obtained from the solutions of equation (7a).

When the conductance parameter approaches zero, the fin is isothermal, and equation (17) reduces to

$$\frac{\frac{Q_b}{Z}}{\sigma T_b^4 \frac{\pi R_o}{2}} = \frac{2}{\pi}\left\{1 + \frac{L}{R_o}\left[1 - \frac{1}{\cos \omega^*} + \frac{1}{\cos \omega^*}\int_0^{1} (F_{X-1} + F_{X-2})dx\right]\right\} \qquad (18)$$

The tube efficiency for this case, however, is not affected by fin taper. The cos ω^* term and the angle-factor expressions, which contain the fin taper and thickness parameters, cancel out numerically for y_o/R_o equal to or less than 0.1.

Figure 6 shows a plot of the tube efficiency as a function of the ratio R_o/L for selected values of N_c and fin taper when the effects of fin thickness, y_o/L, are neglected. For the $N_c = 0$ curve, the $R_o/L = 0$ condition represents the case of a tube with an infinite isothermal central fin. For this situation, the fin occlusion reduces the tube efficiency to 0.818. The other limiting condition of $R_o/L \to \infty$ represents the case of isothermal touching tubes, for which the efficiency approaches $2/\pi$. Tube efficiency increases as the conductance parameter of the fin gets larger, since the fin emits less to the tube because of its reduced temperatures. Fin taper also increases the tube efficiency because tapering reduces the fin temperature profile. As discussed in reference 9, however, these curves should approach the single limiting values of the curve for $N_c = 0$ at $R_o/L = 0$ and ∞. The dashed lines at low values of R_o/L in figure 6 are faired curves.

Consideration of the effects of fin thickness on the tube efficiency indicates that a reduction in efficiency occurs when the fin thickness is increased. This is caused by a reduction in the prime surface area of the tube. The reduction in η_b is less than 2 percent for the case when the ratio of fin thickness to length is 0.1, $R_o/L = 1$, and $N_c = 1$. Even though the tube area reduction is approximately 10 percent at this condition, the effect on the tube efficiency is small since the tube area near the fin contributes little net emission to space because of the occluding effect of the fin.

Total Fin-Tube Heat Rejection

It is desirable to compare the tapered-fin and rectangular-fin radiators on a common basis, that is, the same R_o/L and conductance parameter. It is also important that a fin-tube section of both radiators be compared since variations in fin length and base thickness have marked effects on the heat rejection from the tube or the fin when treated separately. If the definitions of fin efficiency in equation (12) and of tube efficiency in equation (17) are used, the following useful definition of overall fin-tube effectiveness is formulated:

$$\eta_r = \frac{Q_r}{\sigma T_b^4 Z L\left(1 + \frac{R_o}{L}\right)} = \frac{\eta_f + \eta_b \frac{\pi}{2} \frac{R_o}{L}}{1 + \frac{R_o}{L}} \tag{19}$$

Equation (19) is for a quarter section of a tube and a fin, but it is identical to that for an entire fin-tube section of length $2L(1 + R_o/L)$ radiating from two sides.

Figure 7 shows the effectiveness of the entire fin-tube radiator that was obtained by using equation (19) for the case of $y_o/L = 0$. The trends with the taper parameter Y_l and the conductance parameter N_c are in the same direc-

tion as those exhibited by the fin efficiency curves. Factors that reduce the fin thermal resistance improve the overall fin-tube effectiveness. The greatest improvement in radiating effectiveness occurs with increasing R_o/L because more of the radiator is at the base temperature.

The total effectiveness of the fin-tube radiator is equal to 1 for the two limiting cases of $R_o/L = \infty$ and the conductance parameter $N_c = 0$. In both of these cases the entire fin and tube section is isothermal and acts as a blackbody radiator. The total effectiveness approaches the fin efficiency for the third limiting case, $R_o/L = 0$. At this condition, the tube does not contribute to the total radiator effectiveness even though the tube efficiency is finite, as shown in figure 6.

The inclusion of the fin thickness parameter y_o/L resulted in less than a 1-percent variation in total fin-tube effectiveness for $y_o/R_o = 0.1$ at $R_o/L = 1$ and conductance parameters of interest. Thus, within the range of conditions calculated, neglecting the effects of fin thickness on the total radiator heat transfer can generally be justified.

It is also of interest to know what fraction of the overall heat loss is transferred from the fin. A plot of the ratio of fin heat rejection to total radiator heat rejection is presented in figure 8. Inspection of the figure reveals that the fraction of heat lost by the fin is greatest for small values of R_o/L and N_c. The tendency of Q_f/Q_r to increase with decreasing R_o/L is related to the increase in the fin surface area relative to the tube surface area. On the other hand, the changes in Q_f/Q_r with N_c and fin taper are due to changes in the fin temperature distribution.

RADIATOR WEIGHT

The heat-rejection analysis of the fin and the tube was nondimensionalized so that the results could be used for general design purposes. Using the previous results for making a decision as to the merits of employing tapered fins in radiator designs is impractical without consideration of the total weight of the fins and the tubes. It is necessary, therefore, to consider the ratio of heat rejection per unit weight Q/W.

Input information required from the heat-rejection analysis consists of the overall radiator effectiveness (eq. (19)) as a function of N_c, R_o/L, y_l/y_o, and y_o/L. Because of the additional variables of tube internal diameter, meteoroid shield thickness, radiator materials, radiator temperature level, and system power level, weight and area optimizations can be made only for specific cases.

For comparison purposes, it was considered sufficient for the panel geometry to match only the total required heat flow. Consideration of fluid pressure drop and vapor and liquid headers was not included in the formulation of the radiator weight relations. This simplification in essence permits the analysis of a single tube and fin without regard to the number of tubes or to the subsequent individual tube length. A tube-to-tube span is considered in

the thermal analysis, however, so that the radiation interchange between fin and tube is properly included.

Weight Ratio

The heat rejection per unit weight of a fin-tube radiator is given by

$$\frac{Q}{W} = \frac{Q/Z}{W/Z} \tag{20}$$

where, for radiation from both surfaces,

$$\frac{Q}{Z} = \frac{2A^*}{Z}\eta_r\sigma T_b^4 = 2D_o\left(1 + \frac{L}{R_o}\right)\eta_r\sigma T_b^4 \tag{21}$$

For a radiator tube composed of a thin inner liner of thickness δ_c and an armor sleeve of thickness δ_a, the outside tube diameter may be expressed as

$$D_o = D_i + 2\delta_c + 2\delta_a \tag{22}$$

The fin and tube weight per unit length of tube can be calculated by summing the individual weights of the fin, the tube liner, and the tube armor to obtain

$$\frac{W}{Z} = \rho_c\frac{\pi}{4}\left[(D_i + 2\delta_c)^2 - D_i^2\right] + \rho_a\frac{\pi}{4}\left[D_o^2 - (D_i + 2\delta_c)^2\right] + 2\rho_f(1 + Y_l)y_oL \tag{23}$$

When $y_o = \sigma L^2T_b^3/kN_c$ and D_o from equation (22) are introduced into equation (23), the equation for weight per unit length becomes

$$\frac{W}{Z} = \rho_c\pi\delta_c(D_i + \delta_c) + \rho_a\pi\delta_a(D_i + 2\delta_c + \delta_a) + \frac{2\rho_f\sigma T_b^3(1 + Y_l)}{kN_c}\left(\frac{L}{R_o}\right)^3\left(\frac{D_i}{2} + \delta_c + \delta_a\right)^3 \tag{24}$$

Solution of equation (24) for fixed values of N_c, T_b, and Y_l for a given radiator requires input values for the liner and armor thickness. The former is generally prescribed as some function of the tube inside diameter, while the latter depends on the meteoroid protection criterion selected. The tube liner thickness is arbitrarily prescribed as

$$\delta_c = 0.04\ D_i \tag{25}$$

The meteoroid protection criterion used in this analysis is that of reference 10 with revised inputs based on reference 12, as recommended by the authors of reference 10 in a personal communication. According to reference 10, the resultant equation for the armor thickness is

$$\delta_a = 2a\left(\frac{\rho_p\ 62.45}{\rho_a}\right)^{1/2}\left(\frac{\overline{V}_p}{c_a}\right)^{2/3}\left(\frac{6.747\times10^{-5}}{\rho_p}\right)^{1/3}\left(\frac{\alpha A_v \tau}{-\ln P(0)}\right)^{1/3\beta}\left(\frac{1}{\beta+1}\right)^{1/3\beta} \quad (26)$$

where $\beta = 1.34$, $a = 1.75$, $\overline{V}_p = 98{,}400$ feet per second, $\rho_p = 0.44$ gram per cubic centimeter, and $\alpha = 0.53\times10^{-10}$ $g^{3\beta}/(\text{sq ft})(\text{day})$ (Whipple value without Earth shielding). The radiator vulnerable area, taken as the exposed surface area of the tube, is given by

$$A_v = 2D_o Z\left[\frac{\pi}{2} - \sin^{-1}\left(\frac{y_o}{R_o}\right)\right] \quad (27)$$

or, from equation (21),

$$A_v = \frac{Q\left[\frac{\pi}{2} - \sin^{-1}\left(\frac{y_o}{R_o}\right)\right]}{\eta_r \sigma T_b^4\left(1 + \frac{L}{R_o}\right)} \quad (28)$$

The heat-rejection load is related to the cycle power output and overall efficiency by

$$Q_r = 3.413\times10^6\ \mathscr{P}_e\left(\frac{1}{\eta_c} - 1\right) \quad (29)$$

Thus, an iteration solution for W/Z involving equations (19), (26), (28), and (29) is required.

Calculations

Two specific cases are given in order to show the effect of power level, temperature level, and material specification on the radiator heat rejection per unit weight. The first case is a 1-megawatt electrical output powerplant with a 15-percent cycle efficiency and a 1700° R radiator temperature. The tube armor and the fin were assumed to be beryllium, and the tube liner was assumed to be columbium. The second case is a 30-kilowatt system radiating at 1160° R with a 15-percent cycle efficiency. For this case the tube armor and the fin were taken to be aluminum, and the tube liner was taken to be stainless steel. Radiator tube inside diameters of 1/2, 3/4, and 1 inch were used for both cases investigated. A 500-day mission time and a probability of no puncture $P(0)$ of 0.90 were chosen for the calculation of meteoroid protection thickness.

Figures 9 and 10 illustrate the variation of the ratio of total heat rejected to radiator panel weight with fin-tube ratio L/R_o and the conductance parameter N_c for the two examples. The effect of fin tapering in increasing Q/W is most pronounced for large values of L/R_o, where the fin contribution to the total heat transfer is greatest. A peak value of Q/W is attained in all cases. Similar curves are obtained for tube inside diameters of 1/2 and 1 inch.

Plots of maximum values of Q/W against L/R_o for the values of N_c considered are shown in figures 11 and 12 for all three tube inside diameters and fin tapers. At both power levels, fin tapering results in an increase in peak

Q/W of approximately 10 percent for the triangular profile ($Y_1 = 0$). From studies of fins alone (ref. 7), gains of up to 30 percent are indicated. The difference in the case of the radiator panel is explained by noting that the armored radiator tubes account for a sizable portion of the total weight and heat rejection. Thus, the effect of fin tapering on total weight is effectively reduced for the fin and tube configuration.

Peak Q/W occurs at a value of N_c of approximately 1 in all cases considered. The corresponding values of L/R_o for peak Q/W vary somewhat with fin taper and tube diameter at a given power and temperature level. Fin tapering tends to increase the value of L/R_o for peak Q/W. For the 1-megawatt system, the best L/R_o for maximum Q/W varies from approximately 2.5 to 4.0. For the 30-kilowatt system, the best L/R_o increases to values from approximately 5.0 to 8.5.

The 10-percent weight saving indicated in the two examples must be qualified, in that the effects of pressure drop and vapor and liquid header weights were not considered. In effect, the optimum triangular fin is longer than the optimum rectangular fin. Thus, some of the potential weight savings might be offset because the headers for the triangular-fin radiator would be longer and heavier. In this comparison the number of tubes and their length would have to be assumed constant and would be obtained from pressure-drop considerations in the tubes and the headers.

Consideration of the fin-thickness parameter y_o/L in the weight-optimization procedure proved to have very little effect on the heat rejected per unit weight in the vicinity of the design point ($N_c = 1.0$). At some extreme nonoptimum points, a maximum difference of 3 percent or less was obtained.

RADIATOR GEOMETRY

In addition to radiator fin and tube weight, the required planform area of the radiator panel is, in many cases, also of considerable interest with respect to proper integration of the radiator and the space vehicle. Radiator planform area is obtained from equation (21) as

$$A^* = Z(D_o + 2L) = \frac{Q_r}{2\eta_r \sigma T_b^4} \tag{30}$$

Thus, planform area will vary inversely with total fin-tube effectiveness, or, from figure 7, the area will generally increase with increasing L/R_o.

Figures 13 and 14 illustrate the calculated variations of planform area with L/R_o, N_c, and fin taper for the two power cycles for peak Q/W conditions. Fin tapering increases the required planform area for a given value of N_c. Similar results are obtained for the other inside tube diameters.

Other factors of interest with respect to the geometry of the radiator are the fin base thickness and the tube armor thickness. The effect of fin tapering on these factors for a 1/2-inch tube inside diameter is illustrated in figures

15 and 16 for peak Q/W conditions. In both cases, fin tapering results in sizable increases in base thickness and minor reductions in tube armor thickness. Increased fin base thickness may be of advantage with respect to joining or fabrication considerations.

SUMMARY OF RESULTS

From an analysis of the heat-transfer characteristics of fin-tube space radiators with linearly tapered fins (rectangular, trapezoidal, and triangular), it was determined that

1. Fin-tube radiators with tapered fins have lower thermal efficiencies and fin temperature profiles than radiators with rectangular fins.

2. Although fin base thickness and taper angle can have a marked effect on the angle factors between fin and tube, their net effect on the total heat rejection is relatively minor.

Sample calculations of tapered-fin radiators for typical 1-megawatt and 30-kilowatt power systems showed that

1. Tapered fin radiators can be about 10 percent lighter than radiators with fins of constant thickness for the assumptions used for the power cycle and meteoroid protection. The calculation, however, did not include the effects of header weights and fluid pressure drop.

2. Conductance parameters of approximately unity resulted in minimum fin-tube weight for all tapers considered. Corresponding values of the ratio of fin length to tube outside radius varied from 2.5 to 4.0 for the 1-megawatt system to 5.0 to 8.5 for the 30-kilowatt system.

3. Tapered fins are longer and have greater base thicknesses than fins of constant thickness for maximum heat rejection per unit weight.

4. Fin tapering tends to increase radiator planform area at maximum heat rejection per unit weight. Planform area, however, varies most markedly with the ratio of fin length to tube outside radius.

Lewis Research Center
National Aeronautics and Space Administration
Cleveland, Ohio, October 29, 1963

REFERENCES

1. Zipkin, M. A.: Large Turbo-Nuclear Space Power Systems. Presented at Third Symposium on Advanced Propulsion Concepts, Cincinnati (Ohio), Oct. 1961.

2. Evvard, J. C.: Electric Space Propulsion. Electrical Eng., vol. 79, no. 7, July 1960, pp. 555-562.

3. Krebs, Richard P., Winch, David M., and Lieblein, Seymour: Analysis of a Megawatt Level Direct Condenser-Radiator. Paper 2545-62, Am. Rocket Soc., Inc., 1962.

4. Lieblein, Seymour: Analysis of Temperature Distribution and Radiant Heat Transfer Along a Rectangular Fin of Constant Thickness. NASA TN D-196, 1959.

5. Bartas, J. G., and Sellers, W. H.: Radiation Fin Effectiveness. Jour. Heat Transfer (Trans. ASME), ser. C, vol. 82, no. 1, Feb. 1960, pp. 73-75.

6. Mackay, D. B., and Bacha, C. P.: Space Radiator Analysis and Design. TR 61-30, pt. I, Aero. Systems Div., Apr. 1961.

7. Wilkins, J. Ernest, Jr.: Minimum Mass Thin Fins for Space Radiators. Proc. Heat Transfer and Fluid Mechs. Inst., Stanford Univ. Press, 1960, pp. 229-243.

8. Wilkins, J. Ernest, Jr.: Minimum-Mass Thin Fins Which Transfer Heat Only by Radiation to Surroundings at Absolute Zero. Jour. Soc. Ind. Appl. Math., vol. 8, no. 4, Dec. 1960, pp. 630-639.

9. Sparrow, E. M., and Eckert, E. R. G.: Radiant Interaction Between Fin and Base Surfaces. Jour. Heat Transfer (Trans. ASME), ser. C, vol. 84, no. 1, Feb. 1962, pp. 12-18.

10. Loeffler, I. J., Lieblein, Seymour, and Clough, Nestor: Meteoroid Protection for Space Radiators. Paper 2543-62, Am. Rocket Soc., Inc., 1962.

11. Jakab, M.: Heat Transfer, vol. II. John Wiley and Sons, Inc., 1957.

12. Whipple, Fred L.: On Meteoroids and Penetration. Paper Presented at Am. Astronautical Soc. Interplanetary Missions Conf., Los Angeles (Calif), Jan. 1963.

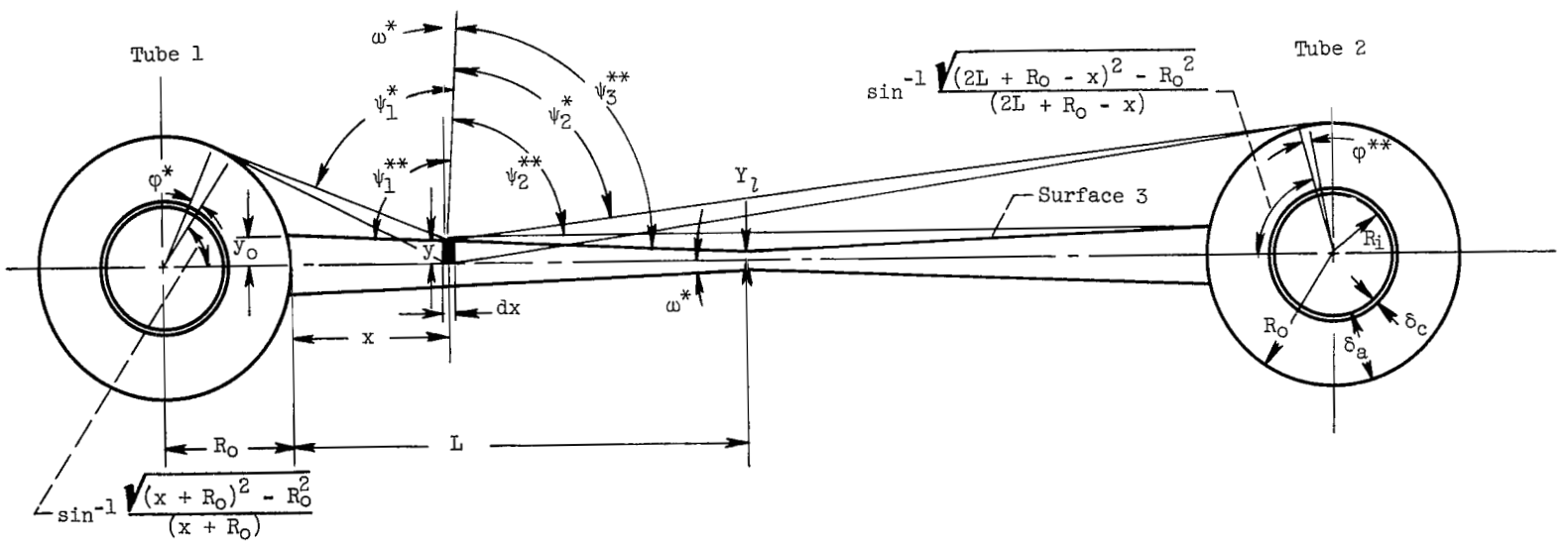

Figure 1. - Tapered-fin - tube configuration.

(a) Rectangular; ratio of fin tip to base thickness, 1.0.

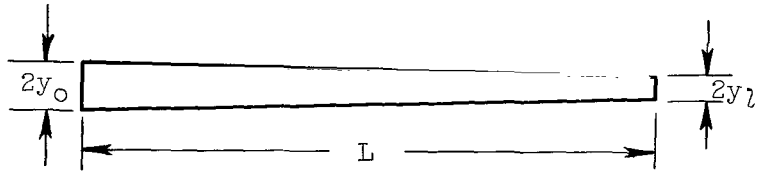

(b) Trapezoidal; ratio of fin tip to base thickness, 0.5.

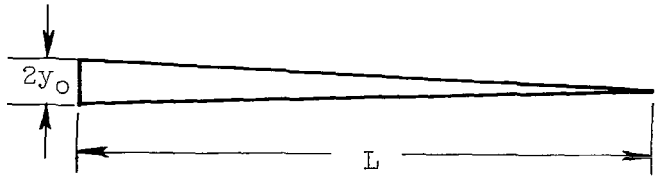

(c) Triangular; ratio of fin tip to base thickness, 0.

Figure 2. - Fin profiles studied.

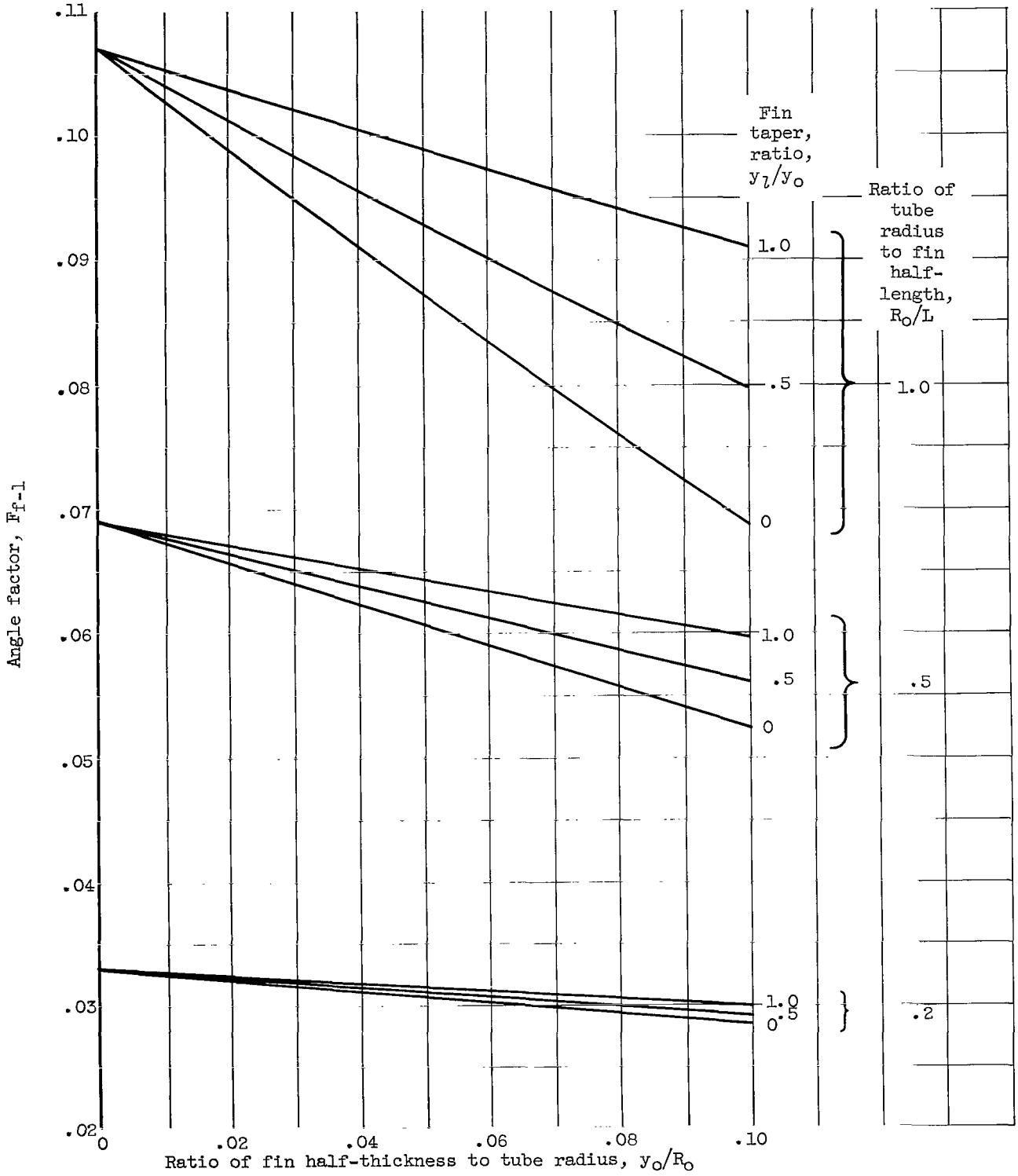

Figure 3. - Effect of fin taper on fin-to-tube view factor.

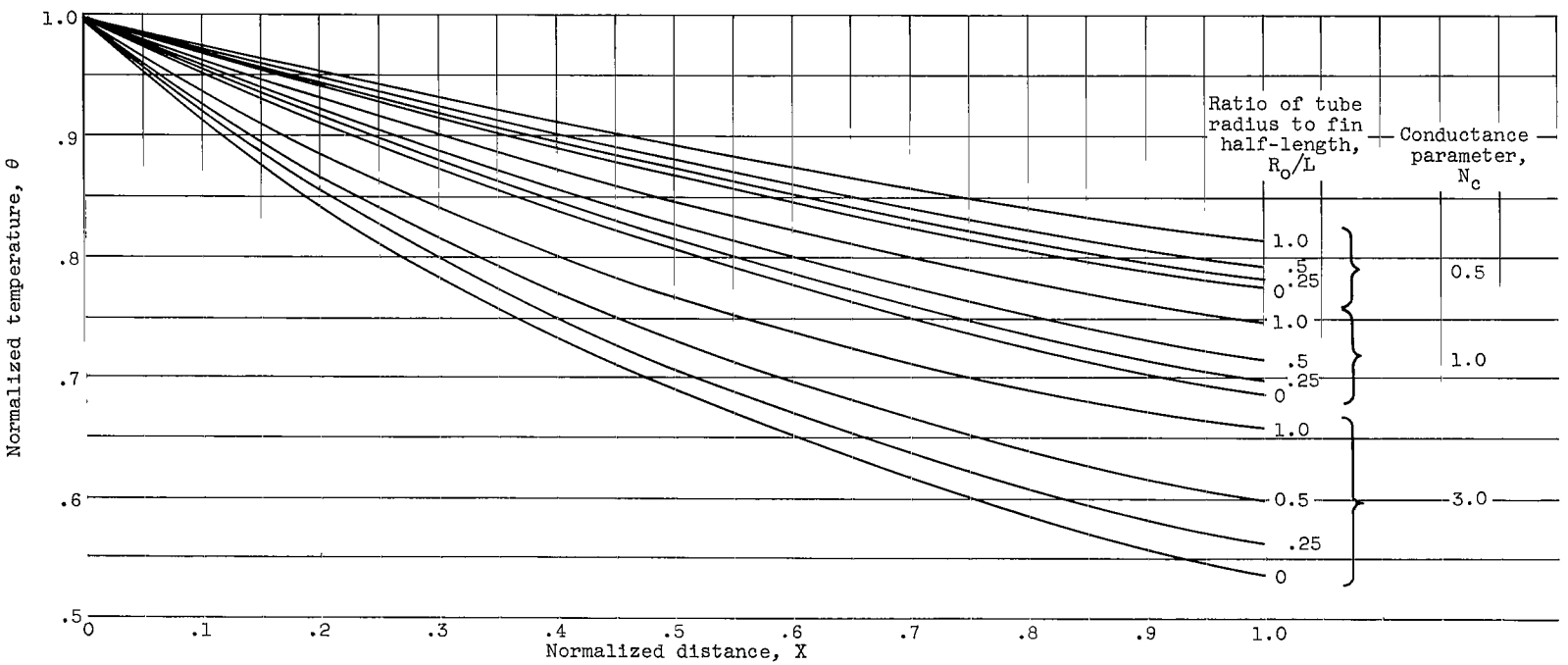

(a) Triangular fin, fin taper ratio, y_l/y_o, 0.

Figure 4. - Fin temperature distribution. Fin thickness ratio, y_o/L, 0.

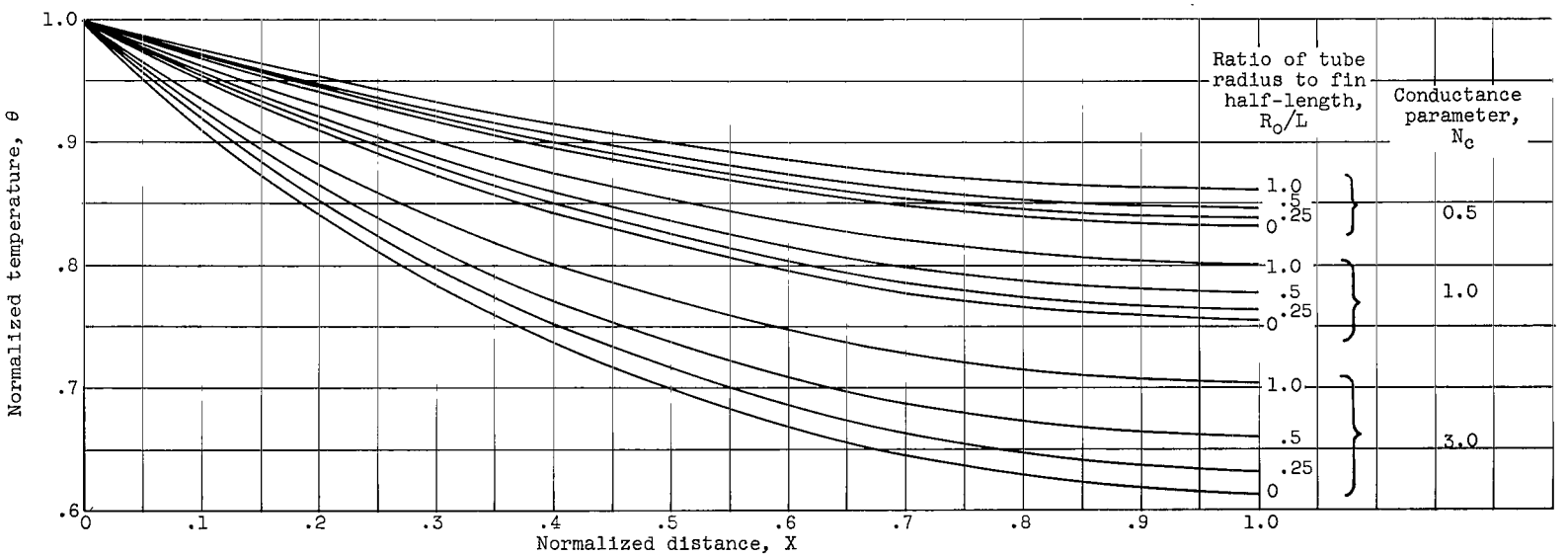

(b) Trapezoidal fin, fin taper ratio, y_l/y_o, 0.5.

Figure 4. - Continued. Fin temperature distribution. Fin thickness ratio, y_o/L, 0.

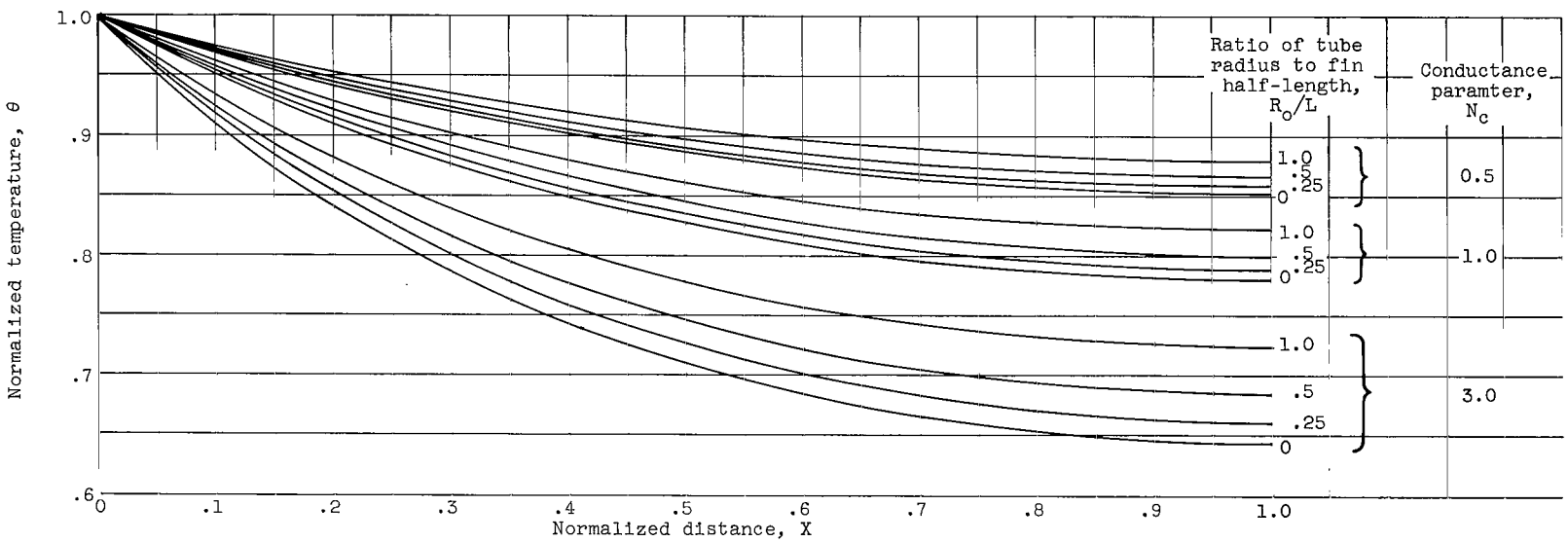

(c) Rectangular fin; fin taper ratio, y_l/y_o, 1.0.

Figure 4. - Concluded. Fin temperature distribution. Fin thickness ratio, y_o/L, 0.

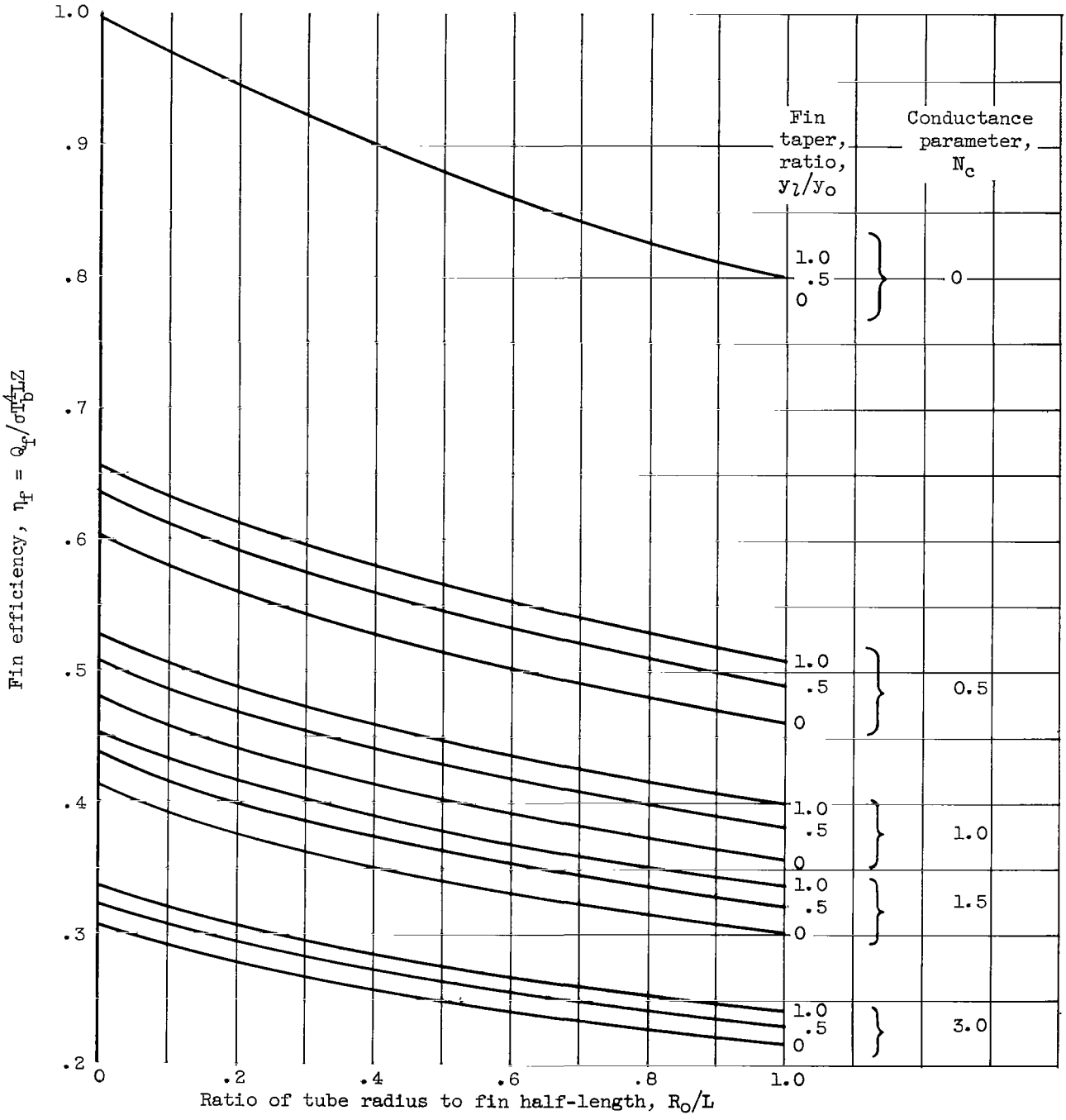

Figure 5. - Fin efficiency as function of ratio of tube radius to fin half-length. Fin thickness ratio, y_o/L, 0.

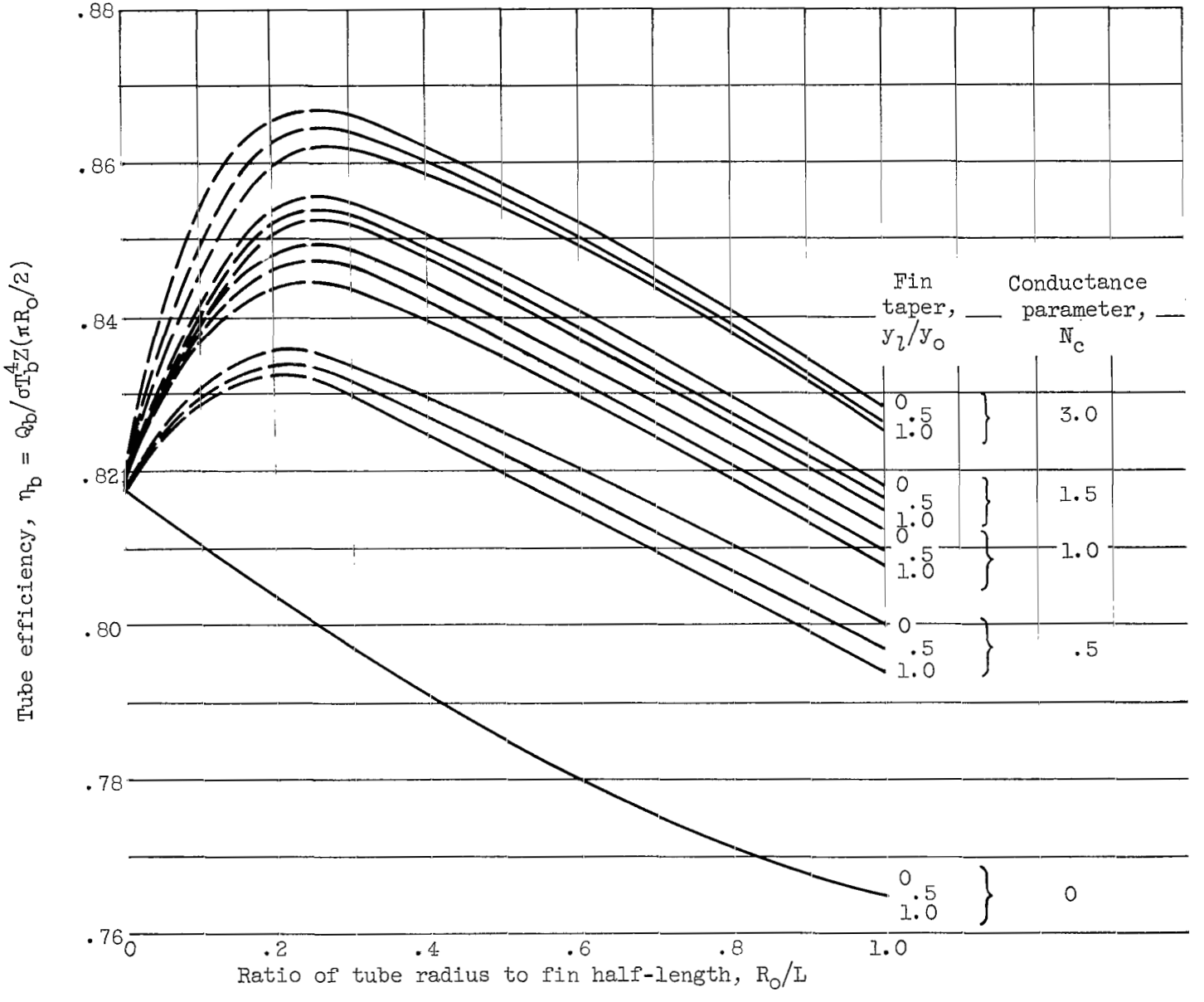

Figure 6. - Tube efficiency as function of ratio of tube radius to fin half-length. Fin thickness ratio, y_o/L, 0.

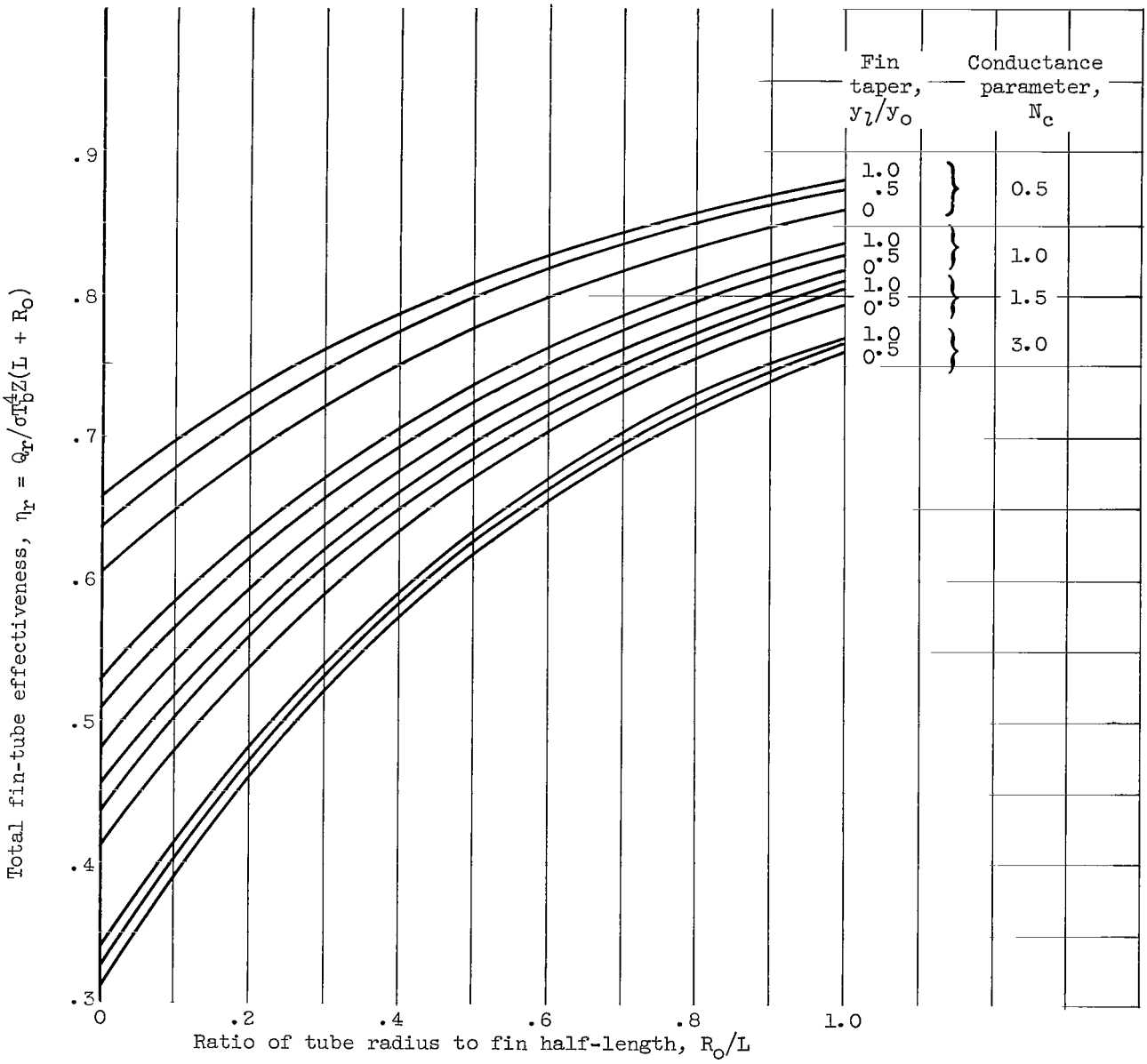

Figure 7. - Total fin-tube effectiveness as function of ratio of tube radius to fin half-length. Fin thickness ratio, y_o/L, 0.

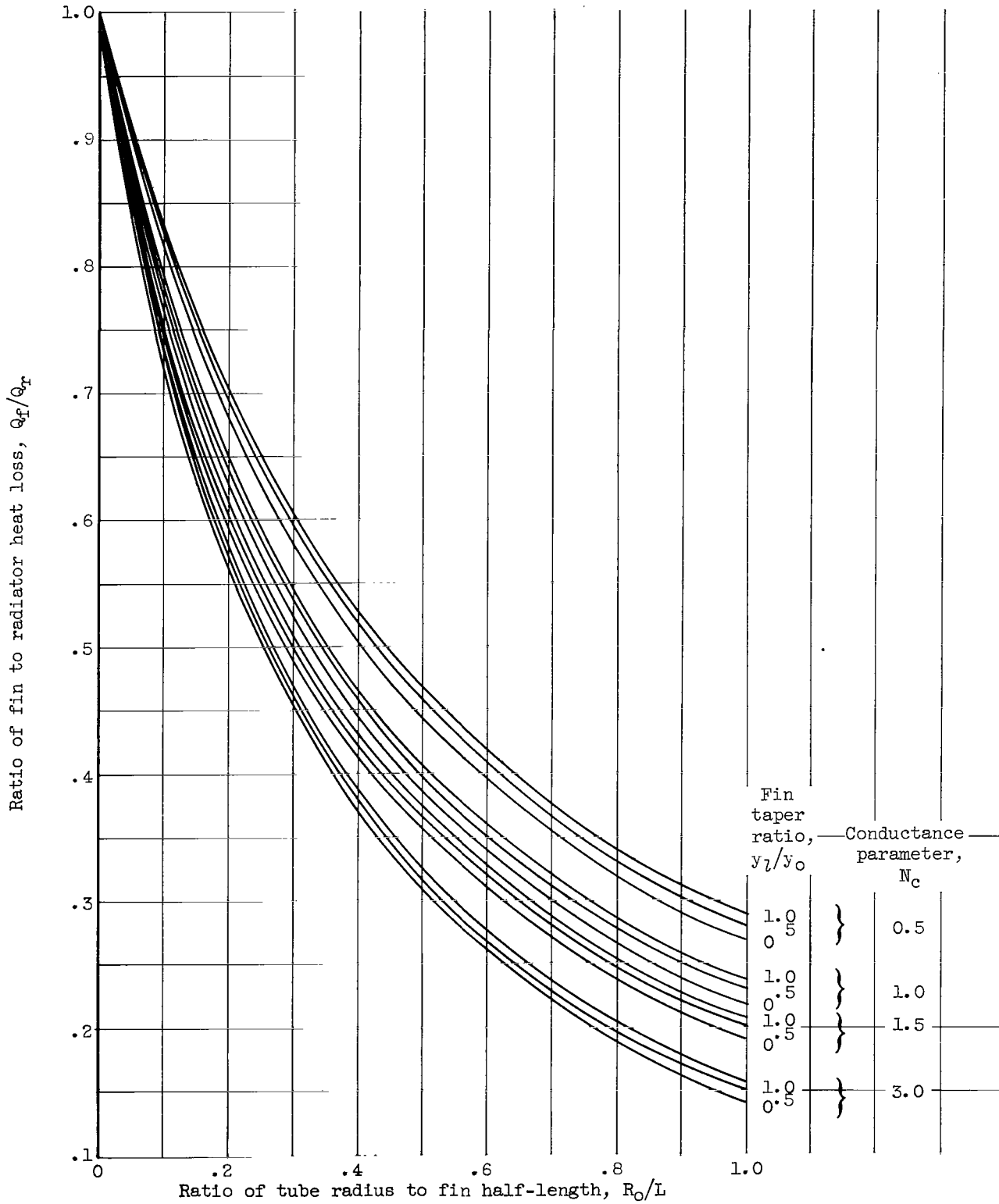

Figure 8. - Fin heat loss relative to total heat loss. Fin thickness ratio, y_o/L, 0.

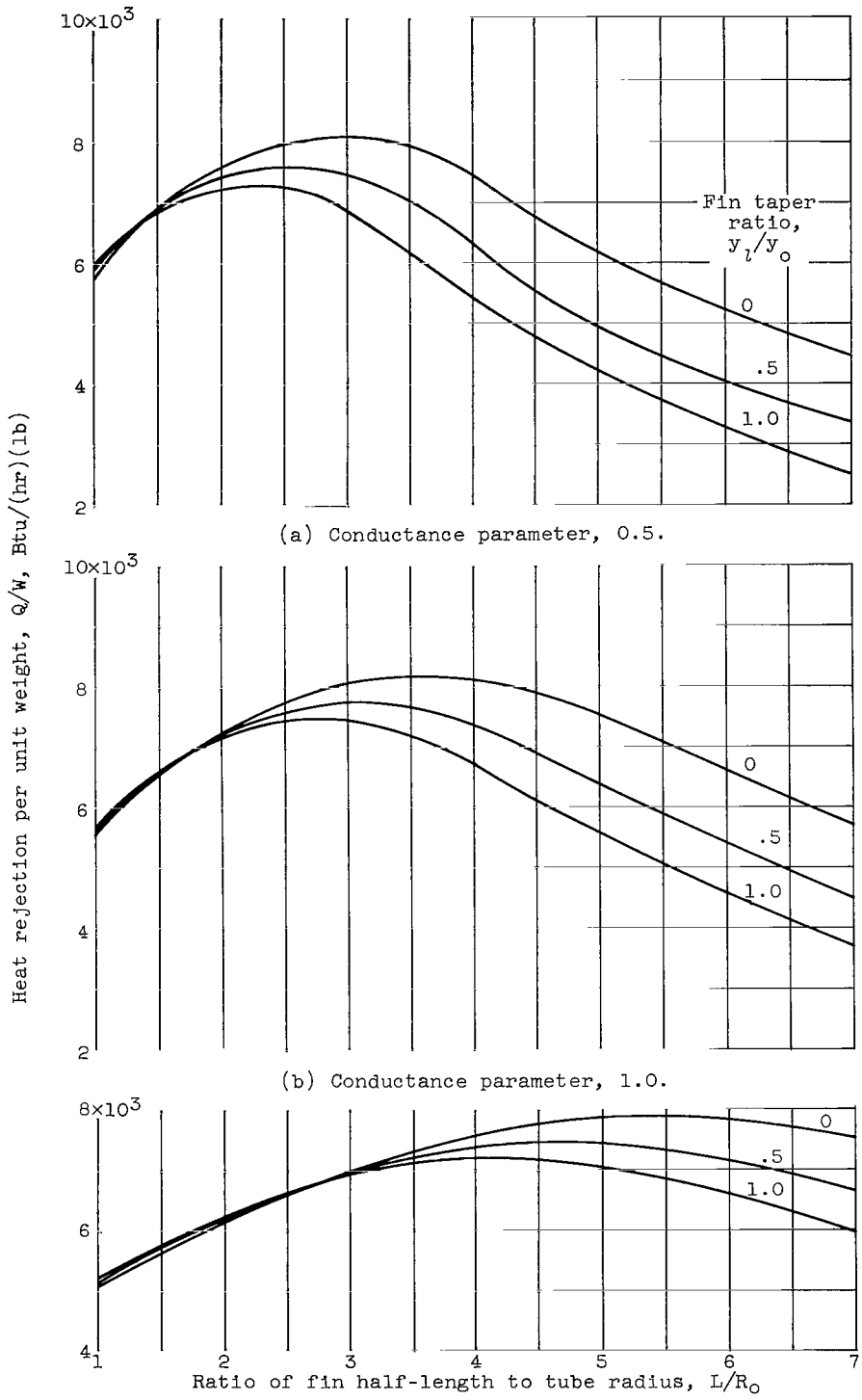

Figure 9. - Ratio of heat rejection to weight for 1-megawatt power system radiating at 1700° R. Beryllium fins and tube armor; tube inside diameter, 3/4 inch.

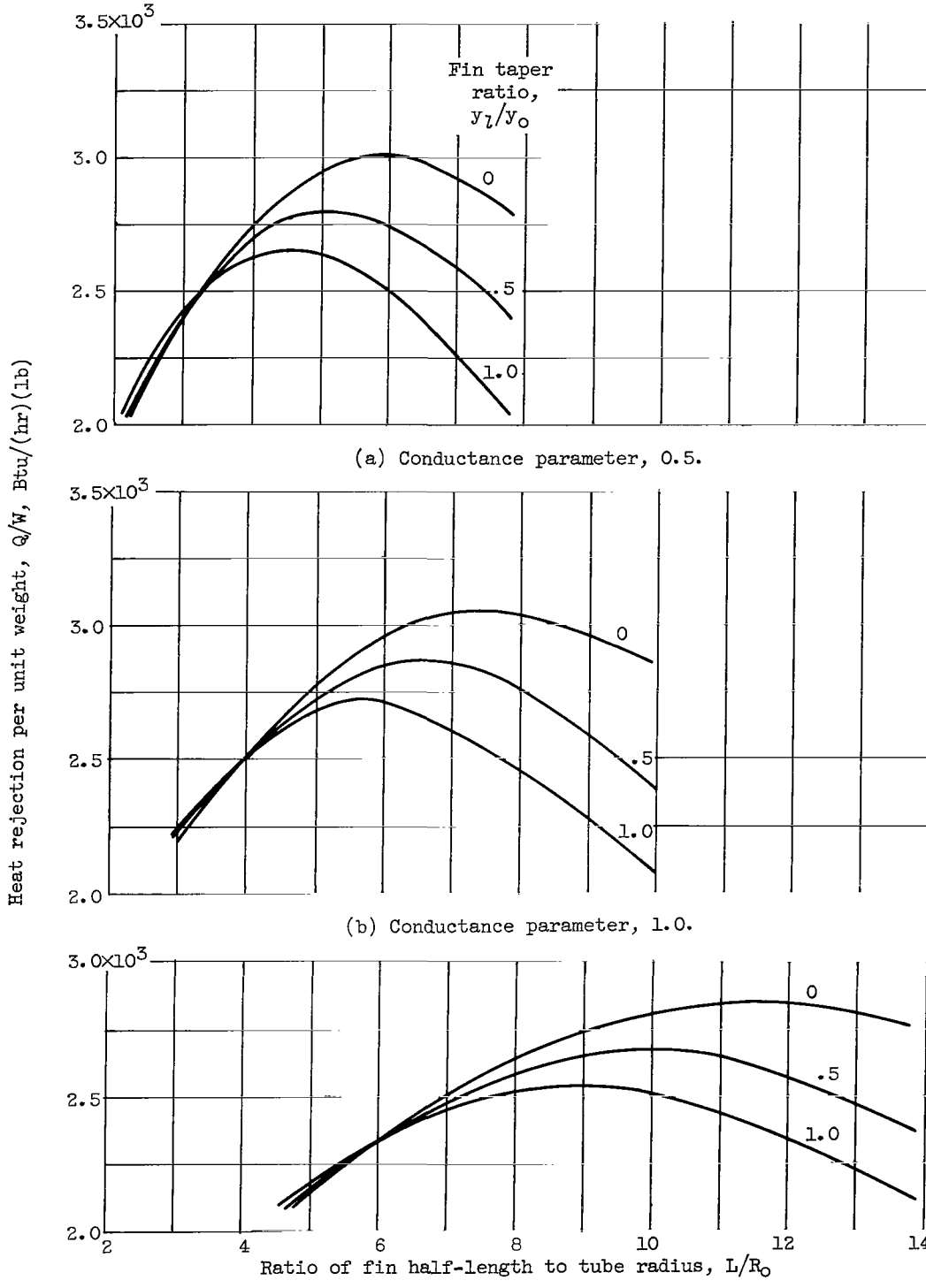

Figure 10. - Ratio of heat rejection to weight for 30-kilowatt power system radiating at 1160° R. Aluminum fins and tube armor; tube inside diameter, 3/4 inch.

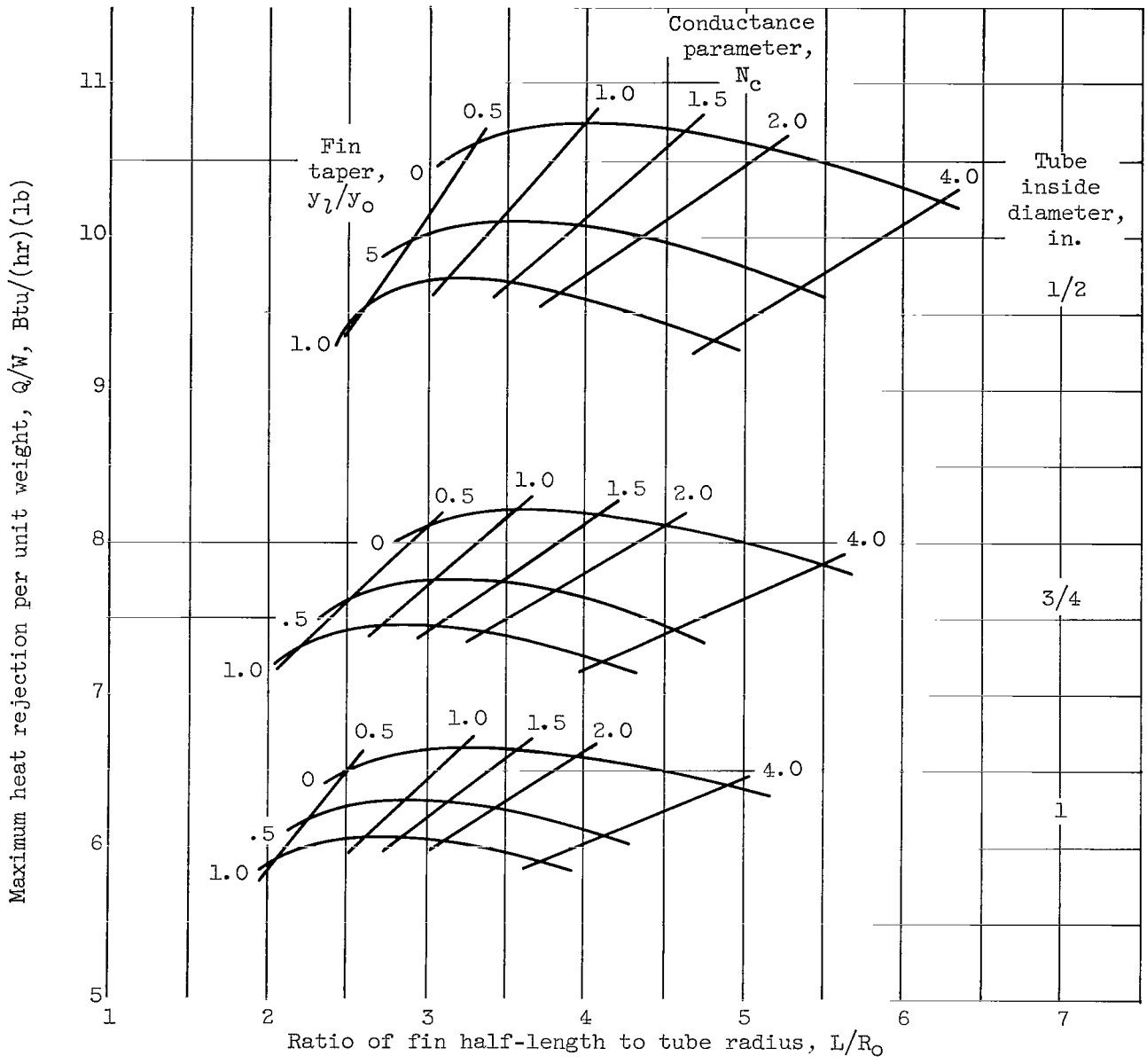

Figure 11. - Radiator performance map for 1-megawatt power system radiating at 1700° R with beryllium fins and tube armor.

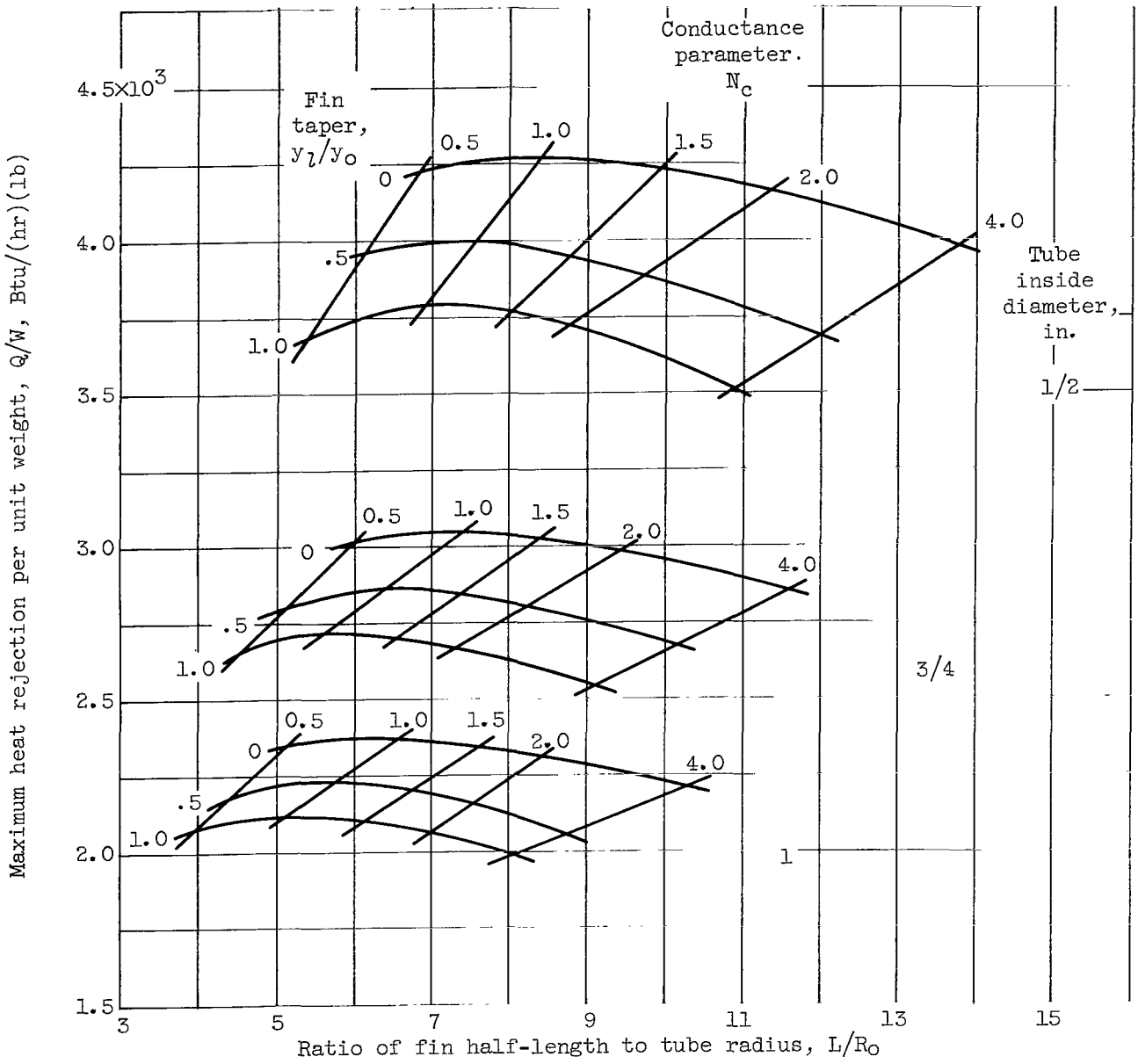

Figure 12. - Radiator performance map for 30-kilowatt power system radiating at 1160° R with aluminum fins and tube armor.

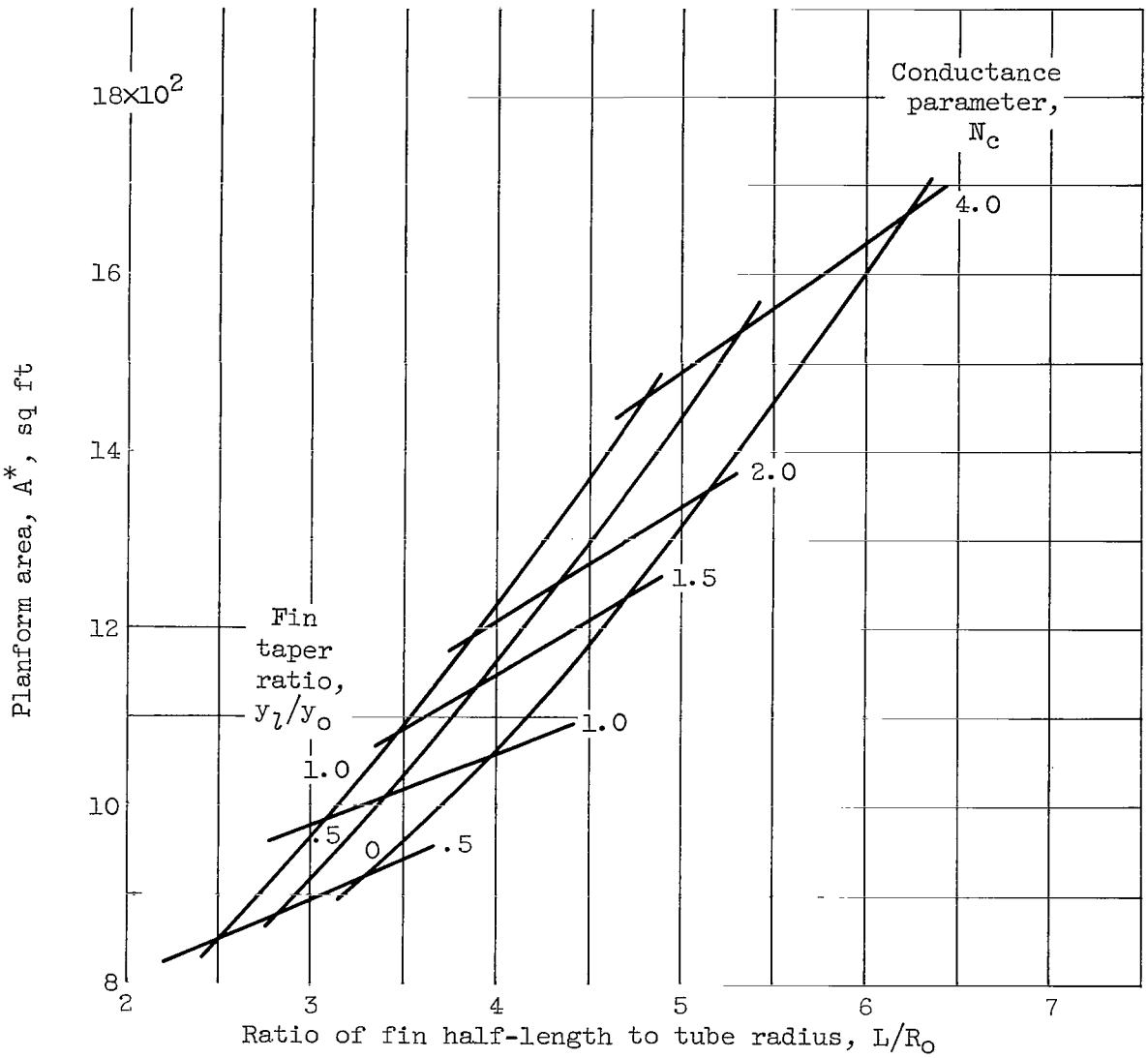

Figure 13. - Radiator planform area requirements for 1-megawatt system radiating at 1700° R. Beryllium fins and tube armor; tube inside diameter, 1/2 inch.

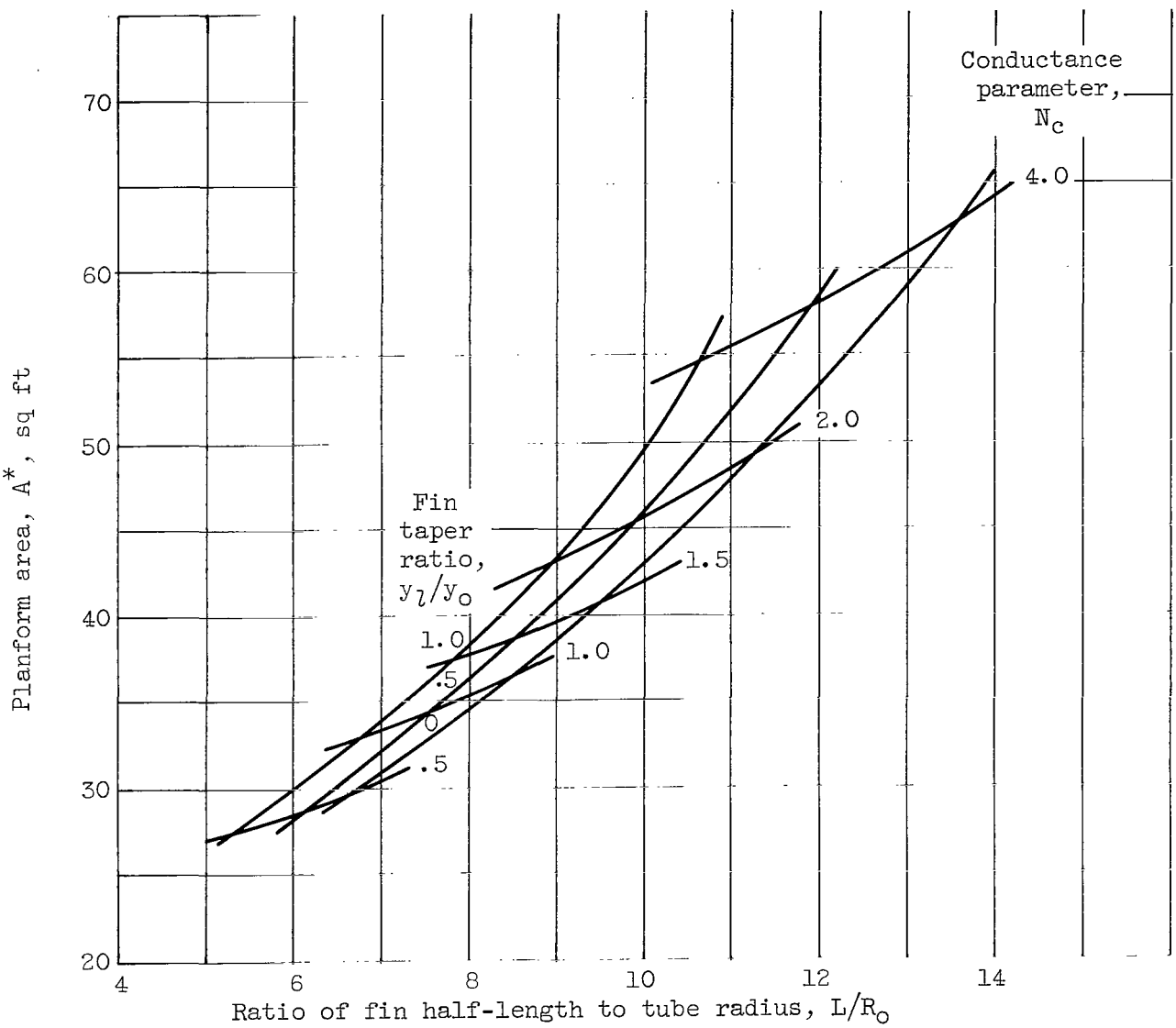

Figure 14. - Radiator planform area requirements for 30-kilowatt power system radiating at 1160° R. Aluminum fins and tube armor: tube inside diameter, 1/2 inch.

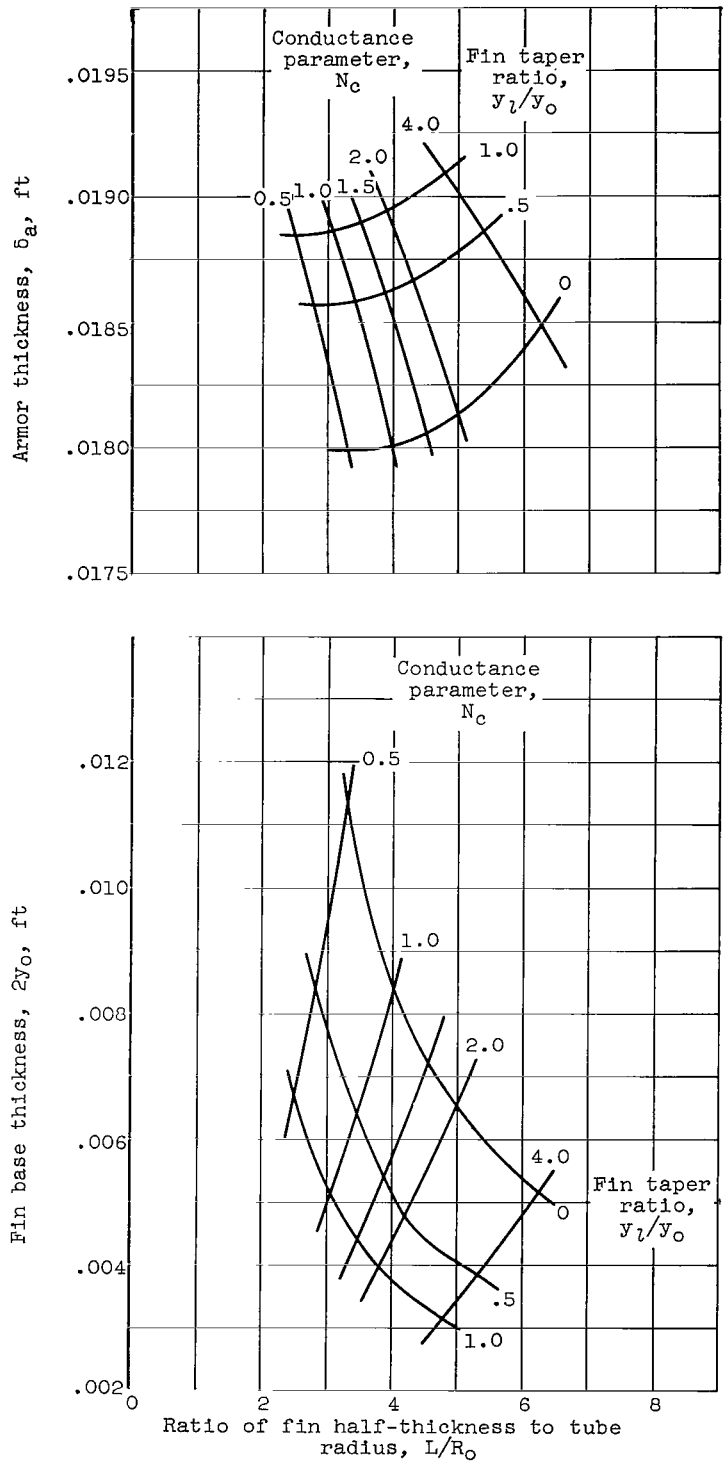

Figure 15. - Radiator physical dimensions for 1-megawatt system radiating at 1700° R. Beryllium fins and tube armor; tube inside diameter, 1/2 inch.

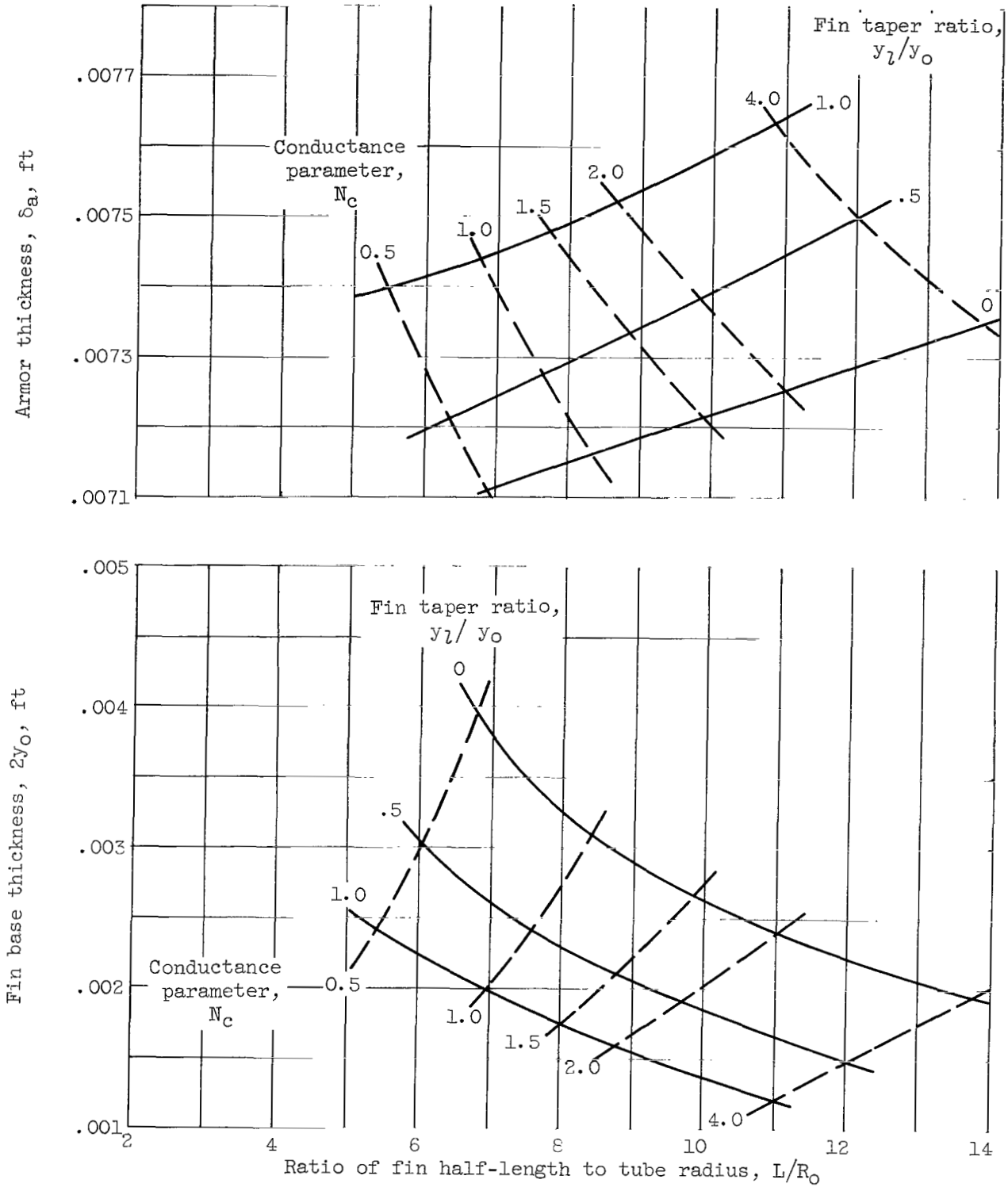

Figure 16. - Radiator physical dimensions for 30-kilowatt power system radiating at 1160° R. Aluminum fins and tube armor; tube inside diameter, 1/2 inch.

NASA-Langley, 1964 E-2182